Spectrochimica Acta Part A 74 (2009) 1197–1203

Contents lists available at ScienceDirect

Spectrochimica Acta Part A: Molecular and Biomolecular Spectroscopy

journal homepage: www.elsevier.com/locate/saa

Molecular structure and vibrational assignments of hippuric acid: A detailed density functional theoretical study

Mehmet Karabacak[a,*], Mehmet Cinar[a], Mustafa Kurt[b]

[a] Department of Physics, Afyon Kocatepe University, 03040 Afyonkarahisar, Turkey
[b] Department of Physics, Ahi Evran University, 40100 Kırsehir, Turkey

ARTICLE INFO

Article history:
Received 20 February 2009
Received in revised form 16 August 2009
Accepted 24 September 2009

Keywords:
Hippuric acid
DFT
Infrared
Raman and NMR spectra
HOMO and LUMO

ABSTRACT

In this study, the structural properties of hippuric acid ($C_9H_9NO_3$, HA) were studied using density functional theory (DFT) employing B3LYP exchange correlation. The geometry of the molecule was fully optimized at B3LYP/6-311G(d,p) level of theory. There are four conformers, C1, C2, C3, and C4 for this molecule. The geometrical parameters and energies have been obtained for all four conformers from DFT. The computational results diagnose the most stable conformer of HA as the C1 form. The vibrational frequencies were calculated and fundamental vibrations were assigned based on the scaled theoretical wavenumbers. The complete assignments were performed on the basis of the total energy distribution (TED) of the vibrational modes, calculated with scaled quantum mechanics (SQM) method. ^{1}H and ^{13}C nuclear magnetic resonance (NMR) chemical shifts of the molecule were calculated by using the gauge-invariant atomic orbital (GIAO) method. A study on the electronic properties, such as HOMO and LUMO energies, were performed by time-dependent DFT (TD-DFT) approach, while taking solvent effects into account. Finally, geometric parameters, vibrational bands, chemical shifts and absorption wavelengths were compared with available experimental data of the molecule.

1. Introduction

Amino acids and their compounds with different metal ions play an important role in biology, pharmacy and industry [1]. Hippuric acid (HA) namely N-benzoyl-glycine or benzoylaminoacetic acid, is a colorless crystal obtained from the urine of domestic animals and also in smaller amounts in human urine [2]. HA's quantification in urine has the disadvantage of showing great variation in and between individuals, depending on environmental and individual factors [3]. For instance, toluene is metabolized into HA and excreted in the urine of humans exposed to toluene. However, exposure to toluene may result in central nervous system depression and decreased memory [4]. Thus, HA quantification in urine actually is mainly used as a diagnostic marker of exposure to toluene [5].

Liebig [6] is the first who discovered hippuric acid which was isolated from equine urine and in contrast to benzoic acid, it contains nitrogen. The second harmonic generation (SHG) behavior and NLO (non-linear optical) properties of HA crystal was studied by several workers [7–9]. Urinary HA determination has been performed by several methods such as high-performance liquid chromatography (HPLC) and gas chromatographic methods [10–12], ^{1}H NMR spectroscopy [13], capillary electrophoresis [14–17], isotachophoresis [18] and also capillary micellar electrokinetic chromatography (MEKC) [19,20]. The X-ray crystallographic structure of HA was determined by Ringertz [21] and recently by Kacar [22]. Refat et al. [23] reported the Mn(II), Au(III) and Zr(III) complexes with HA that synthesized and characterized by elemental analysis, molar conductivity, magnetic measurements, spectral methods and simultaneous thermal analysis techniques.

However, as we know, no DFT studies have been made on the conformation and spectroscopic behaviors of the HA. Theoretical investigations can facilitate the solution to the problems confronted in the experimental techniques that is, allowing the determination of the minima energy and the optimal geometric structure. Hence, this study has been undertaken to study the molecular structure, vibrational and electronic transitions, and NMR chemical shifts. We have carried out DFT calculations with the combined Becke's three-parameter exchange functional in combination with the Lee, Yang and Parr correlation functional (B3LYP) exchange-correlation energy functions. The geometric structure, vibrational frequencies, ^{1}H and ^{13}C NMR chemical shifts, HOMO–LUMO energies, absorption wavelengths, excitation energies, electric dipole moment (μ) of HA were studied. A detailed interpretation of the vibrational spectra of HA has been made on the basis of the calculated total energy distribution (TED).

* Corresponding author. Tel.: +90 272 2281311; fax: +90 272 2281235.
E-mail address: karabacak@aku.edu.tr (M. Karabacak).

1386-1425/$ – see front matter © 2009 Elsevier B.V. All rights reserved.
doi:10.1016/j.saa.2009.09.035

2. Quantum chemical calculations

The first task for the computational work was to determine the optimized geometry of the compound. The spatial coordinate positions of HA, as obtained from an X-ray structural analysis [22], were used as the initial coordinates for the theoretical calculations. The B3LYP method based on Becke's three-parameter functional [24,25] of DFT yields a good description of harmonic vibrational wavenumbers for small and medium sized molecules. Therefore, we choose this method to calculate harmonic vibrational wavenumbers with 6-311G(d,p) basis set. The stability of the optimized geometries was confirmed by frequency calculations, which give positive values for all the obtained frequencies. However, the frequency values computed at these levels contain known systematic errors [26]. Therefore, these values were scaled by 0.9668 [27]. The total energy distribution (TED) was calculated by using the SQM [28] program and the fundamental vibrational modes were characterized by their TED.

For NMR calculations, the title molecule was firstly optimized and after optimization, ^{1}H and ^{13}C NMR chemical shifts (δH and δC) were calculated using the GIAO method in dimethylsulfoxide (DMSO) and gas phase at B3LYP method with 6-311G(d,p) basis set [29,30]. Relative chemical shifts were then estimated by using the corresponding TMS shielding calculated in advance at the same theoretical level as the reference. ^{13}C and ^{1}H isotropic magnetic shielding (IMS) of any X carbon (or hydrogen) atom was made according to the value ^{1}H or ^{13}C IMS of TMS: (H or C)$S_x = IMS_{TMS} - IMS_x$. The electronic properties have also been calculated using two different methods; B3LYP and PBE1PBE of the time-dependent DFT (TD-DFT) [31–34], basing on the optimized structure. All calculations are performed by using Gausssian 03 program package on the personal computer [35].

3. Results and discussion

Hippuric acid is a monocarboxylic acid with three types of donor site: the nitrogen and the oxygen atom of the carboxylic acid group, and the oxygen atoms of the amide group. Hippuric acid may have four possible structures in connection with the hydrogen orientations of the oxygen atom of the carboxylic acid group. Calculated energies and energy difference of four structures for title molecule are presented in Table S1 (supporting information). From DFT calculations, the conformer C1 is predicted to be from 2.897 to 15.259 kcal/mol more stable than the other conformers. We tabulated only C1 conformer calculations data because of most stable conformer.

The molecule of HA consists of 22 atoms, so it has 60 normal vibrational modes. On the basis of C_S symmetry the 60 fundamental vibrations of title compound can be distributed as 41 in-plane vibrations of A′ species and 19 out of plane vibrations of A″ species. i.e., $\Gamma_{vib} = 41A' + 19A''$. All the 60 fundamental vibrations are active in both IR and Raman. In the C1 form of molecule are non-planar structure and have the C1 symmetry and the vibrational modes span the irreducible representations: 60A.

3.1. Molecular geometry

The insolubility of the compounds in both polar and non-polar solvents would suggest that they have polymeric structures and so a complete structure determination of these compounds cannot be made. As mentioned previously, HA have four possible structures. Our calculations show that the four structures for HA, do not differ greatly in energy, but demonstrate that structure C1 has the lowest energy and the most stable one. Fig. 1 shows the optimized structure and demonstration of four possible conformations

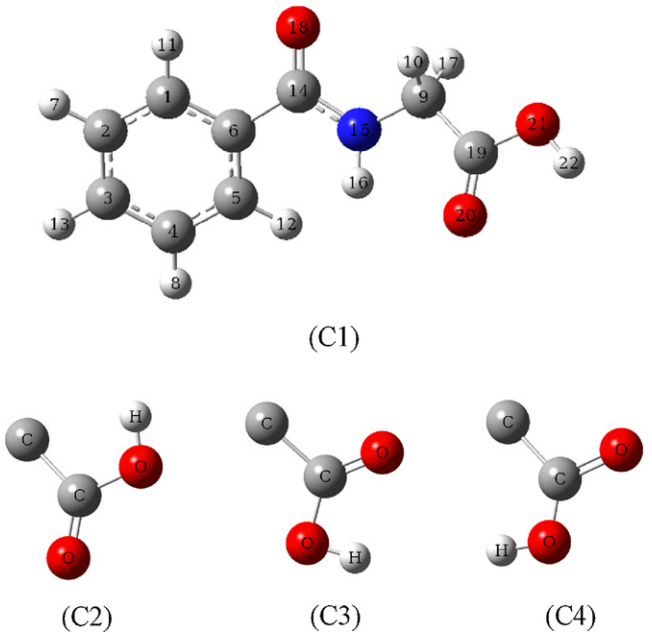

Fig. 1. The theoretically optimized four possible geometric structures with atoms numbering of hippuric acid.

of compound along with numbering of the atoms. The optimized geometrical parameters of HA calculated by B3LYP with the 6-311G(d,p) basis set are listed in Table 1 in accordance with the atom numbering scheme given in Fig. 1. The available experimental bond lengths, bond angles, selected dihedral angles and intramolecular hydrogen bonds determined by X-ray crystallography are also listed for comparison [22].

From the theoretical values one can find that most of the optimized bond lengths are larger than the experimental values, due to that the theoretical calculations belong to isolated molecules in gaseous phase and the experimental results belong to molecule in solid state. For this compound there are three main planes which are ring plane, C1–C2–C3–C4–C5–C6 (I), O18–N15–C6–C14–C9 (II) and O20–O21–C9–C19 (III). The ring plane (I) makes dihedral angles of 14.06° and 81.96° with the II and III planes, respectively. The dihedral angle between II and III is 84° [22]. As shown in Fig. S1 the molecular structure has three intramolecular hydrogen bonds of the type N–H···O, O–H···O and C–H···O. The experimental and calculated results are given in Table 1. The predicted angle of C–H···O is bigger 20° than experimental result. Other parameters are close to each other.

3.2. Vibrational analysis

The fundamental wavenumbers of HA as calculated by DFT using 6-311G(d,p) basis set are given in Table 2. The resulting vibrational wavenumbers for the optimized geometry as well as IR intensities, Raman scattering activities and available experimental IR wavenumbers [23] are also given in the table. The simulated IR and Raman spectra at 6-311G(d,p)/B3LYP level of theory are shown in Fig. 2 where the calculated intensities and scattering activities are plotted against the harmonic vibrational wavenumbers. It should be noted that calculations were made for a free molecule in vacuum, while experiments were performed for solid samples. Furthermore the anharmonicity is neglected in real system for calculated vibrations. Thus, there are disagreements between calculated and observed vibrational wavenumbers, and some frequencies are calculated, however these frequencies are not observed in the IR spectrum, as seen in Table 2. In the last column is given a detailed

Table 1
Comparison of the theoretical and experimental geometric parameters for C1 conformer of HA, bond lengths in angstrom, angles in degrees.

Bond lengths (Å)	X-ray [22]	B3LYP	Bond angles (°)	X-ray [22]	B3LYP
C(1)–C(2)	1.390	1.390	C(2)–C(1)–C(6)	119.9	120.4
C(1)–C(6)	1.390	1.398	C(2)–C(1)–H(11)	118.4	121.4
C(1)–H(11)	0.980	1.084	C(6)–C(1)–H(11)	121.6	118.2
C(2)–C(3)	1.370	1.395	C(1)–C(2)–C(3)	120.2	120.1
C(2)–H(7)	1.000	1.084	C(1)–C(2)–H(7)	115.4	119.9
C(3)–C(4)	1.377	1.393	C(3)–C(2)–H(7)	124.4	120.1
C(3)–H(13)	0.960	1.084	C(2)–C(3)–C(4)	120.3	119.9
C(4)–C(5)	1.389	1.392	C(2)–C(3)–H(13)	118.0	120.1
C(4)–H(8)	0.980	1.084	C(4)–C(3)–H(13)	121.7	120.0
C(5)–C(6)	1.387	1.400	C(3)–C(4)–C(5)	120.1	120.1
C(5)–H(12)	0.960	1.084	C(3)–C(4)–H(8)	122.9	120.1
C(6)–C(14)	1.497	1.503	C(5)–C(4)–H(8)	116.9	119.8
C(9)–H(10)	0.968	1.096	C(4)–C(5)–C(6)	120.0	120.3
C(9)–N(15)	1.447	1.443	C(4)–C(5)–H(12)	119.8	119.0
C(9)–H(17)	0.970	1.095	C(6)–C(5)–H(12)	120.2	120.6
C(9)–C(19)	1.500	1.511	C(1)–C(6)–C(5)	119.4	119.2
C(14)–N(15)	1.327	1.366	C(1)–C(6)–C(14)	117.2	117.3
C(14)–O(18)	1.240	1.223	C(5)–C(6)–C(14)	123.4	123.5
N(15)–H(16)	0.900	1.010	H(10)–C(9)–N(15)	108.8	111.5
C(19)–O(20)	1.192	1.206	H(10)–C(9)–H(17)	105.0	105.9
C(19)–O(21)	1.326	1.345	H(10)–C(9)–C(19)	111.0	109.3
O(21)–H(22)	0.990	0.969	N(15)–C(9)–H(17)	109.4	111.9
Selected dihedral angles (°)			N(15)–C(9)–C(19)	113.6	109.4
C(6)–C(14)–N(15)–C(9)	177.9	176.9	H(17)–C(9)–C(19)	109.0	108.8
O(18)–C(14)–N(15)–C(9)	2.5	3.2	C(6)–C(14)–N(15)	118.4	116.4
C(4)–C(5)–C(6)–C(14)	177.5	179.4	C(6)–C(14)–O(18)	120.2	122.1
N(15)–C(9)–C(19)–O(21)	174.2	178.2	N(15)–C(14)–O(18)	121.4	121.5
C(1)–C(6)–C(14)–O(18)	13.2	17.0	C(9)–N(15)–C(14)	121.7	120.4
C(5)–C(6)–C(14)–O(18)	165.4	161.6	C(9)–N(15)–H(16)	114.0	116.0
C(1)–C(6)–C(14)–N(15)	167.2	163.1	C(14)–N(15)–H(16)	125.0	121.5
C(5)–C(6)–C(14)–N(15)	14.2	18.2	C(9)–C(19)–O(20)	126.1	125.1
C(2)–C(1)–C(6)–C(14)	177.9	179.8	C(9)–C(19)–O(21)	109.7	111.4
N(15)–C(9)–C(19)–O(20)	6.1	1.9	O(20)–C(19)–O(21)	124.2	123.6
			C(19)–O(21)–H(22)	109.1	107.1
N(15)–H(16)···O(18)	Exp. [22]	B3LYP	O(21)–H(22)···O(18)	Exp. [22]	B3LYP
N–H	0.90	1.02	O–H	0.93	0.99
H···O	2.15	1.93	H···O	1.77	1.74
N–H···O	162°	167°	O–H···O	162°	169°
C(5)–H(12)···O(18)	Exp. [22]	B3LYP			
C–H	0.96	1.08			
H···O	2.53	2.40			
C–H···O	165°	146°			

description of the normal modes based on the total energy distribution (TED). All of the calculated modes are numbered from the smallest to the biggest frequency within each fundamental wavenumbers, in the first column of the table.

It is stated that the N–H stretching vibrations occur in the region 3200–3500 cm^{-1} and O–H stretching band is characterized near about 3400–3600 cm^{-1} [36]. As seen in Table 2 there is one peak observed for HA in the 3300–4000 cm^{-1} range experimentally which is ca. 3342 cm^{-1}. This peak had been assigned as N–H stretching [7,9,23]. We calculated this peak at 3489 cm^{-1}. In this range the vibration modes 59 and 60 were assigned N–H and O–H stretching, respectively. As expected these two modes are pure stretching modes as it is evident from TED column, they are almost contributing 100%.

The high frequency region above 3000 cm^{-1} is the characteristic region for the ready identification of C–H stretching vibrations [36]. In the present study, the five adjacent hydrogen atoms left around the ring give rise five C–H stretching modes (54–58),

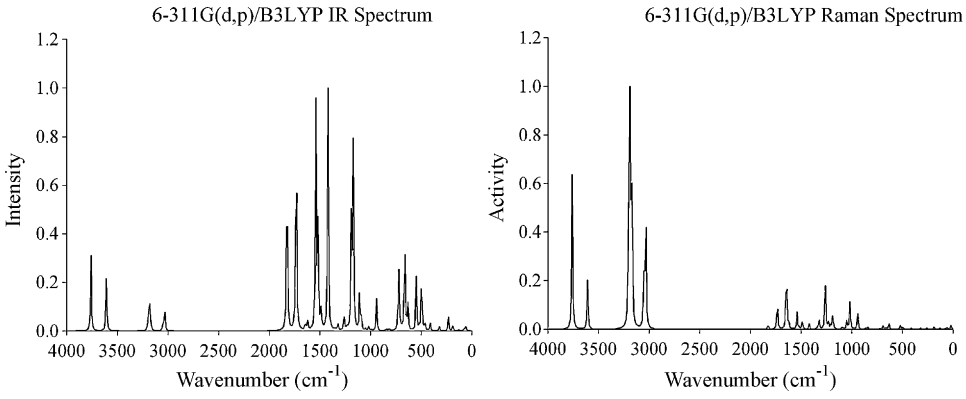

Fig. 2. The simulate IR and Raman spectra of HA.

Table 2
Comparison of the calculated and experimental vibrational spectra of HA.

Mode no.	B3LYP/6311G(d,p)				Experimental			
	Unscaled freq.	Scaled freq.[a]	$I^{Infrared}$	S^{Raman}	Exp. [23]	Exp. [7]	Exp. [9]	TED (%)
1	20	19	0.17	4.28				τCNCH(35) + τCNCC(35) + τCCCN(11)
2	51	49	0.14	0.61				tCOOH(59) + τCCCO(18) + τCCNC(12)
3	63	60	5.55	1.58				τCCCN(31) + τCCCO(10) + τHNCH(10)
4	76	74	2.31	0.88				δCCN(32) + δCNC(20) + {τCCCN + τCCCO}(12)
5	127	123	1.52	1.45				τCCCC(20) + $\delta CH_2(20)_{rock.}$ + τNCCO(15)
6	187	181	6.41	2.62				τCCCC(30) + δCCN(15) + τCNCO(10) + δCCC(10)
7	231	223	15.64	0.62				δCCC(30) + {δCNC + τHNCO + τHNCH}(10)
8	262	253	0.06	1.69				δCNC(19) + νC–COOH(18) + νCN(17) + νCC(10)
9	321	311	4.77	1.37				δCCO(40) + δNCO(20) + νCC(10)
10	410	397	7.6	1.18				τCCNH(53) + $\tau CCCC(19)_{ring}$ + δCCO(14) + νCC(10)
11	416	402	1.2	0.07				$\tau CCCC(53)_{ring}$ + $\tau CCCH(24)_{ring}$
12	463	448	9.6	0.75		436	430	$\tau CCCC(24)_{ring}$ + δCCO(15) + $\tau CCCH(10)_{ring}$
13	496	480	68.88	2.57		476		γNH(57) + γOH(16) + $\delta CH_2(10)_{rock}$
14	521	503	2.6	3.79				γOH(32) + γCH(29) + $\delta CH_2(27)_{rock}$
15	549	531	60.02	0.53		545	535	δCCO(33) + δCCN(15) + δOCO(12)
16	632	611	29.49	2.33				δOCO(30) + δCCO(27) + $\nu CCC(10)_{ring}$
17	634	613	4.47	5.73				$\delta CCC(53)_{ring\ def.}$ + δOCO(12) + δCCO(10)
18	663	641	112.14	1.58	632 ring def.	630		τOCOH(60) + τCCOH(20) + $\delta CH_2(10)_{rock}$
19	689	666	1.58	3.63	661 ring def.	660	652	$\delta CCC(40)_{ring}$ + νCC(12) + δCCN(10)
20	706	683	5.2	0.14	690 ring def.			$\tau CCCC(54)_{ring}$ + $\gamma CH(30)_{ring}$
21	723	699	84.33	1.09	696 ring def.	692		$\gamma CH(60)_{ring}$ + τCCCO(13) + τCNCO(11)
22	816	788	2.98	0.69		723	713	$\gamma CH(25)_{ring}$ + {τNCCC + τCCCO}(15) + τCCNC(12)
23	843	815	1.99	2.45	851 νCC	850	851	νCC(50) + δNCO(13) + δCOH(10)
24	863	834	0.77	1.42				$\gamma CH(82)_{ring}$ + $\tau CCCC(16)_{ring}$
25	941	910	36.78	17.06	880 νCC			νCC(27) + δNCO(14) + δCNC(12)
26	947	916	1.3	0.98				$\gamma CH(80)_{ring}$
27	991	958	0.82	0.22	943 νCC	945		$\gamma CH(85)_{ring}$
28	1014	980	0.33	1.14				$\gamma CH(80)_{ring}$
29	1018	984	3.31	5.65	1000 CH_2 rock	1000	1012	$\delta CH_2(39)_{rock}$ + $\delta CCC(12)_{ring}$
30	1018	984	1.37	27.46				$\nu CC(29)_{ring}$ + $\delta CH_2(22)_{rock}$ + $\delta CCC(17)_{ring}$
31	1049	1014	1.99	9.38	1031 CH_2 rock	1028		$\nu CC(50)_{ring}$ + $\delta CCC(15)_{ring\ breat.}$ + $\delta CH(12)_{ring}$
32	1094	1057	18.34	2.89				νCN(31) + $\nu CC(27)_{ring}$ + $\delta CH(15)_{ring}$
33	1109	1072	40.25	0.14	1080 CH_2 rock	1079		$\delta CH(27)_{ring}$ + $\nu CC(25)_{ring}$ + νCN(15)
34	1172	1133	223.95	0.47				νCO(31) + {νCN + δCOH}(19)
35	1183	1144	1.54	5.39				$\delta CH(77)_{ring}$ + νCC(17)
36	1189	1150	116.85	11.73				νCN(28) + δCH(13) + {νCC + νCO + δCOH}(10)
37	1207	1167	0.17	4.78	1185 δCH	1182 δCCOO	1175	$\delta CH(60)_{ring}$ + $\nu CC(21)_{ring}$
38	1233	1192	3.47	8.55				$tCH_2(75)$ + τHCCO(14)
39	1263	1221	17.78	59.72				δCNH(28) + νCN(15) + νCC(14)
40	1322	1278	7.45	11.04	1259 νCC	1258		δCOH(20) + νCO(10) + νCC(10)
41	1335	1290	0.88	1.57	1304 δCH_2			$\nu CC(62)_{ring}$ + δCH(21)
42	1353	1308	1.66	0.8	1318 δCH_2	1314	1319	$\delta CH(72)_{ring}$ + $\nu CC(28)_{ring}$
43	1421	1373	263.92	5.4	1336 δCH_2	1354		$\delta C–CH_2(16)$ + νCO(16) + νCC(14) + δCOH(13)
44	1477	1428	3.51	2.17		1395 δCH_2	1406	$\delta CH(50)_{ring}$ + $\nu CC(30)_{ring}$
45	1490	1441	18.83	7.02	1448 δCH_2	1416 δCH_2		$\delta CH_2(80)$ + τOCCH(20)
46	1518	1468	123.48	1.94				$\delta CH(45)_{ring}$ + $\nu CC(20)_{ring}$ + δCNH(16)
47	1540	1489	245.28	18.33	1492 CH def.	1490 νCC + νCN		δCNH(34) + νCN(20) + δCCH(10)
48	1622	1569	11.24	5.79	1607 δNH	1556 νCC (ring)	1566 νCC_{ring}	$\nu CC(68)_{ring}$ + $\delta CCH(14)_{ring}$
49	1645	1590	8.44	79.26	1621 δNH	1604 νCC (ring)		$\nu CC(67)_{ring}$ + $\delta CCH(16)_{ring}$
50	1734	1677	258.4	36.47	1745 νCO	1744 νCO	1613 νCO	νCO(81)
51	1825	1764	222.78	6.04	1760 νCO		1749 νCO	νCO(85)
52	3033	2933	28.27	148.63				$\nu CH_2(100)_{sym.}$
53	3053	2952	6.25	66.96	2940 νCH	2938 νCH of CH_2		$\nu CH_2(100)_{asym.}$
54	3163	3058	1.16	38.33				$\nu CH(100)_{ring}$
55	3171	3065	5.1	117.81				$\nu CH(100)_{ring}$
56	3180	3074	24.81	58.38	3075			$\nu CH(100)_{ring}$
57	3190	3084	15.66	221.07	3087	3090 νOH	3082 νOH	$\nu CH(100)_{ring}$
58	3203	3097	5.06	131.35				$\nu CH(100)_{ring}$
59	3608	3489	61.62	56.92	3342 νNH	3342 νNH	3344 νNH	νNH(100)
60	3760	3635	81.28	164.65				νOH(100)

ν; stretching, δ; in-plane bending, γ; out-of-plane bending, τ; torsion, t; twisting.

[a] Scale factor of 0.9668 was used for B3LYP/6-311G(d,p) basis set [27] [Frequency (cm^{-1}), IR intensities; $I^{Infrared}$ (K m/mol), Raman scattering activities; S^{Raman} (Å amu^{-1})].

five C–H in plane bending (35, 37, 42, 44, 46) and five C–H out-of-plane bending (21, 24, 26–28) vibrations. Accordingly, five calculated values appear that correspond to ring C–H stretching vibrations in the range of 3058–3097 cm^{-1}. They are very pure modes since their TED contribution are 100%. The C–H in-plane bending frequencies appear in the range of 1000–1300 cm^{-1} and C–H out-of-plane bending vibration in range of 750–1000 cm^{-1} [37]. Both in plane and out-of-plane C–H bending vibrations were assigned in the range that mentioned above and according to the calculated TED, they are described as mixed modes. After scaling procedure, the theoretical C–H vibrations are in good agreement with experimental values and the literature [7,9,23,38]. The change in the frequencies of these deformations from the values in benzene is almost determined exclusively by the relative position of the substituent and is almost independent of their nature [39].

The asymmetric stretching for the CH_2, NH_2, and CH_3 has magnitude higher than the symmetric stretching [38]. The antisymmetric and symmetric CH_2 stretching appears strongly at ca. 2926 and 2853 cm^{-1} in IR and Raman [38]. The asymmetric CH_2 stretch (mode 53) calculated with B3LYP after scaling down gives the value of 2952 cm^{-1}, shows agreement with experimental value [7,23]. The symmetric stretch of CH_2 (mode 52) was calculated at 2933 cm^{-1} while this vibration was not observed in IR spectra [7,9,23]. According to the calculated TED, our calculations show that there are pure stretching vibrations of CH_2. The scissoring mode of the CH_2 group gives rise to a characteristic band near 1465 cm^{-1} in IR and Raman spectra [38]. In the present investigation, the calculated vibrational frequency of 1441 cm^{-1} is in good agreement with observed value of 1448 cm^{-1} [23] and this vibration was assigned as CH_2 scissoring (mode 45).

The band observed in the 1700–1800 cm^{-1} region is due to the C=O stretching vibration which is one of the characteristic feature of carboxylic acid group. With reference to this, the vibrational frequencies described by modes 50 and 51 assigned to the C=O stretching modes. These vibrations were observed at 1745 and 1760 cm^{-1} by Refat et al. [23]. Vijayan et al. [7] observed one vibration (1714 cm^{-1}) and Bhat and Dharmaprakash [9] observed two values at 1613 and 1749 cm^{-1} for this vibration mode.

The ring stretching vibrations are very important in the spectrum of benzene and its derivatives are highly characteristic of the aromatic ring itself. Vibrations between 1400 and 1650 cm^{-1} in benzene derivates are assigned ring carbon–carbon stretching modes. In this study, the CC stretching modes are calculated at 1569 and 1590 cm^{-1} (modes 48 and 49) which observed at 1556 and 1604 cm^{-1} in the IR spectrum [9]. As revealed by TED, the ring-breathing mode which can be described as the 'trigonal ring breathing' vibration or the 'star of David' vibration of the aromatic ring at 1014 cm^{-1} coincides satisfactorily with the IR band at 1028 cm^{-1} [9]. The C–N stretching frequency is a rather difficult task since there are problems in identifying these frequencies from other vibrations. The C–N stretching is observed at 1490 cm^{-1} [9]. After scaled down computed value (mode 47) of C–N stretching vibration also is 1489 cm^{-1} near to the observed one. The TED for this mode suggests that this is a mixed mode. All present assignments agree well with the values available in the literature [7,9,23,36–41].

3.3. NMR spectra

The isotropic chemical shifts are frequently used as an aid in identification of reactive ionic species. It is recognized that accurate predictions of molecular geometries are essential for reliable calculations of magnetic properties. Therefore, molecular structure of the hippuric acid was optimized by using B3LYP method in conjunction with 6-311G(d,p). Then, GIAO ^{13}C and ^{1}H chemical shift calculations of the compound has been made by using same method and basis set. The B3LYP method allows calculating the shielding constants with the proper accuracy, and the GIAO [29,30] method is one of the most common approaches for calculating nuclear magnetic shielding tensors. The NMR spectra calculations were performed for gas phase and in dimethylsulfoxide (DMSO) solvent. The isotropic shielding values were used to calculate the isotropic chemical shifts δ with respect to tetramethylsilane (TMS). Besides X-ray crystallography, ^{1}H NMR spectroscopy can provide the required structural data for the investigated compound [22,23]. Theoretical and experimental chemical shifts of HA in ^{1}H and ^{13}C NMR spectra are gathered in Table 3. Taking into account that the range of ^{13}C NMR chemical shifts for a typical organic molecule usually is >100 ppm [42,43], the accuracy ensures reliable interpretation of spectroscopic parameters. In the present paper, ^{13}C NMR chemical shifts in the ring are >100 ppm, as they would be expected. Due to the electronegative property of oxygen atom, the chemical shift value of C14 and C19 which has bigger value than the others, have calculated at 169.0 and 176.2 ppm, respectively (C=O). Similarly, six carbons peaks in the ring are calculated from 129.5 to 137.3 ppm. Besides, other carbon peak is calculated 42.7 ppm (C–N). ^{1}H atom is the smallest of all atoms and is mostly localized on periphery of the molecules; therefore their chemical shifts would be more susceptible to intermolecular interactions in the aqueous solutions as compared to that for other heavier atoms.

Table 3
^{1}H and ^{13}C isotropic chemical shifts (with respect to TMS, all values in ppm) for HA.

Atom	Exp. [23]	Gas	DMSO	Atom	Gas	DMSO
H(7)	7.53	7.51	7.83	C(1)	134.0	132.4
H(8)	7.40	7.40	7.80	C(2)	132.2	132.7
H(10)	3.99	4.29	4.31	C(3)	134.9	136.8
H(11)	7.91	8.29	8.27	C(4)	131.1	132.6
H(12)	7.53	7.55	7.93	C(5)	128.1	129.5
H(13)	7.53	7.49	7.90	C(6)	138.1	137.3
H(16)	8.63	5.91	6.30	C(9)	42.9	42.7
H(17)	3.99	3.90	4.01	C(14)	166.9	169.0
H(22)	12.50	5.71	7.58	C(19)	174.5	176.2

The formation of hydrogen bonds leads to a significant downfield shift of the isotropic chemical shifts. If hydrogen-bond formation involves amide protons and the carbonyl group, the direction of the electron density shift from the NH to the carbonyl group results in a decreased magnetic shielding for the amide proton and hence results in a shift to lower field of its proton signal [44,45]. Therefore, the experimental chemical shift value of H16 (8.63 ppm) is smaller than H22 (12.5 ppm). In this study, there is good agreement between experimental and theoretical chemical shift results.

3.4. Electronic properties

The charge distributions are often altered significantly in the presence of a solvent reaction field. We have examined the Mulliken atomic charges both in gas phase and in solution. The results are shown in Table S2. The charge distributions are influenced by a dielectric medium, as expected. To investigate the computational method effects, we have selected two methods of TD-DFT, B3LYP and PBE1PBE, using with 6-31G(d) basis set. If we consider the gas phase results, it may be noted that the carbon atom C(19) has a large net positive charge of 0.559 Debye (D) and the oxygen atoms O(18), O(20) and O(21) have large net negative charge of −0.525, −0.459, −0.560 D. Similarly, charge of nitrogen atom N(15) is −0.649 D. As seen in Table 3 all the hydrogen atoms have a net positive charge; in particular, the hydrogen atoms H(16) and H(22) that have charge of 0.486 and 0.537 D, respectively. The presence of large amounts of negative charge on mentioned oxygen and N(15) atoms, and net positive charge on H(16) and H(22) atoms may suggest the presence of both inter-molecular as well as intra-molecular hydrogen bonding in the crystalline phase.

Both the highest occupied molecular orbital (HOMO) and the lowest unoccupied molecular orbital (LUMO) are the main orbital taking part in chemical reaction. The HOMO energy characterizes the ability of electron giving, the LUMO characterizes the ability of electron accepting, and the gap between HOMO and LUMO characterizes the molecular chemical stability [46]. The energy gap between the HOMOs and LUMOs, is a critical parameter in determining molecular electrical transport properties because it is a measure of electron conductivity. These results are illustrated in Table 4. Surfaces for the frontier orbitals were drawn to understand the bonding scheme of present compound. We examine the four important molecular orbitals (MO) for HA: the second highest

Table 4
Calculated energies, dipole moments and frontier orbital energies.

Atom	TD-DFT/B3LYP		TD-DFT/PBE1PBE	
	Gas $\varepsilon_r = 1$	DMSO $\varepsilon_r = 46.7$	Gas $\varepsilon_r = 1$	DMSO $\varepsilon_r = 46.7$
E_{total} (Hartree)	−628.82963174	−628.85217249	−628.12794825	−628.15153109
E_{HOMO} (eV)	−0.24835	−0.25361	−0.26061	−0.26542
E_{LUMO} (eV)	−0.03339	−0.03622	−0.02937	−0.03296
ΔE (eV)	0.21496	0.21739	−0,23124	0.23246
E_{HOMO-1} (eV)	−0.25420	−0.25494	−0.26512	−0.26676
E_{LUMO+1} (eV)	−0.00650	−0.00527	−0.00108	−0.00147
μ (D)	2.4711	3.4543	2.4782	3.4502

Table 5
Calculated and experimental absorption wavelength λ, excitation energies *E*, and oscillator strengths (*f*).

Exp. [23]	B3LYP						PBE1PBE						
	Gas			DMSO			Gas			DMSO			
λ (nm)	λ (nm)	*E* (eV)	*f*	λ (nm)	*E* (eV)	*f*	λ (nm)	*E* (eV)	*f*	λ (nm)	*E* (eV)	*f*	Assignment [23]
235	224	5.52	0.0027	228	5.45	0.3154	219	5.66	0.1929	223	5.67	0.3340	π–π* transition
245	240	5.17	0.0059	242	5.13	0.114	235	5.27	0.0067	234	5.23	0.123	π–π* transition
262	266	4.65	0.1631	255	4.87	0.006	260	4.77	0.0028	249	4.98	0.0061	n–π* transition

and highest occupied MOs and the lowest and the second lowest unoccupied MOs which we denote HOMO−1, HOMO, LUMO and LUMO+1, respectively. These MOs are outlined in Fig. 3. According to Fig. 3, the HOMO of free HA presents a charge density localized mainly on the ring, C–N and C=O double bond and LUMO is characterized by a charge distribution on all carbon atoms of ring and N–H bond.

The lowest singlet → singlet spin-allowed excited states of HA were taken into account for the TD-DFT calculation in order to investigate the properties of electronic absorption. The calculations were performed for gas phase and dimethylsulfoxide (DMSO) solvent. It is necessary to consider the solvent effects because the spectral data available were obtained in DMSO [23]. The calculated absorption wavelengths (λ) and excitation energies (*E*) of the HA are reported in Table 5 along with oscillator strengths. For a comparison, experimental wavelengths are also given in Table 5. There are six detected absorption bands at 215, 235, 245, 262, 285 and 323 nm in the spectrum of the free ligand. The first three bands are all caused by the π–π* [23,47] and the second three bands are all caused by the n–π * intraligand transitions [23,48,49], respectively [23]. The TD-DFT method gives slightly overestimated values. The deviation between experiment and theory may be resulted from solvent effects. Solvent make the chemical environment of molecule in the simulation become very complex. The calculated values of the electric dipole moment μ (in Debye) are also presented in Table 5.

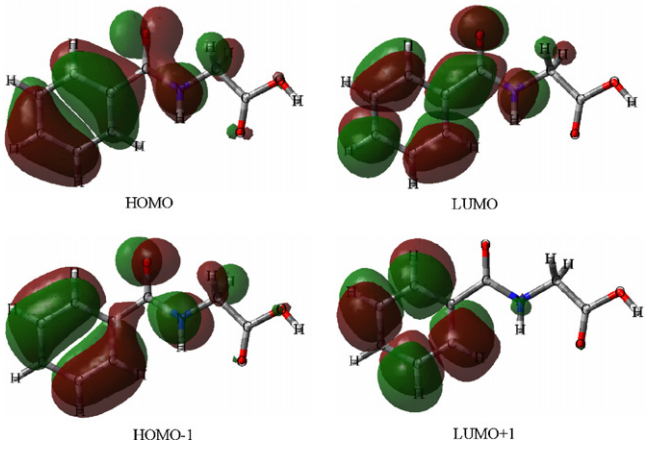

Fig. 3. The HOMO, second HOMO, LUMO and second LUMO distribution of hippuric acid by using B3LYP.

4. Conclusion

In the present study, the geometric structure, vibrational frequencies, ^{1}H and ^{13}C NMR chemical shifts of Hippuric acid were studied using DFT (B3LYP) calculations with the 6-311G(d,p) basis set. A study on the electronic properties of compound has been performed by both B3LYP and PBE1PBE method. The absorption wavelengths (λ), excitation energies and oscillator strengths (*f*) were calculated in gas phase and DMSO solvent. On the basis of the calculated results; assignment of the fundamental vibrational frequencies has been examined. The available experimental results were compared with theoretical data.

Acknowledgement

We thank Dr. Tahir Güllüoglu for SQM program Ahi Evran University, Kırsehir, Turkey.

Appendix A. Supplementary data

Supplementary data associated with this article can be found, in the online version, at doi:10.1016/j.saa.2009.09.035.

References

[1] N. Sewald, H.D. Jakube, Peptides: Chemistry and Biology, Wiley-VCH Verlag Gmb H&Co, KGaA, 2002.
[2] B.L. Oser, Hawk's Physiological Chemistry, 14th edn, Tata McGraw-Hill, New Delhi, 1976.
[3] A. Temellini, S. Mogavero, P.C. Giulianotti, A. Pietrabissa, F. Mosca, G.M. Pacifici, Xenobiotica 23 (1993) 1427.
[4] O. Axelson, Current Aspects of Solvent Related Disorders in Developments in Occupational Medicine, Yearbook Medical Publishers Inc, Chicago, 1977.
[5] C.M. Jone, A.H. Wu, Clin. Chem. 34 (1988) 2596.
[6] J. Liebig, Poggendorff's Ann. Phys. Chem. 17 (1829) 389.
[7] N. Vijayan, R.R. Babu, R. Gopalakrishnan, P. Ramasamy, M. Ichimura, M. Palanichamy, J. Cryst. Growth 273 (2005) 564.
[8] N. Vijayan, G. Bhagavannarayana, A.M.Z. Slawin, Mater. Lett. 62 (2008) 2480.
[9] M.N. Bhat, S.M. Dharmaprakash, J. Cryst. Growth 243 (2002) 526.
[10] R. Tardif, J. Brodeur, G.L. Plaa, J. Anal. Toxicol. 13 (1989) 313.
[11] S. Kira, Br. J. Ind. Med. 34. (1977) 305.
[12] P. Kongtip, J. Vrarussami, V. Pruktharathikul, J. Chromatogr. B 751 (2001) 199.
[13] C. Zuppi, I. Messana, F. Forni, C. Rossi, L. Pennacchietti, F. Ferrari, B. Giardina, Clin. Chim. Acta 265 (1997) 85.
[14] T. Wessel, C. Lanvers, S. Fruend, G. Hempel, J. Chromatogr. A 894 (2000) 157.

[15] M. Shirao, R. Furuta, S. Suzuki, H. Nakazawa, S. Fujita, T. Maruyama, J. Chromatogr. A 680 (1994) 247.
[16] T. Fujii, S. Kawabe, T. Horike, T. Taguchi, M. Ogata, J. Chromatogr. B 730 (1999) 41.
[17] P. Simon, T. Nicot, J. Chromatogr. B 679 (1996) 103.
[18] J. Sollenberg, J. Chromatogr. 545 (1991) 369.
[19] K.J. Lee, J.J. Lee, D.C. Moon, Electrophoresis 15 (1994) 98.
[20] C. Zuppi, D.V. Rossetti, A. Vitali, F. Vincenzoni, B. Giardina, M. Castagnola, I. Messana, J. Chromatogr. B 793 (2003) 223.
[21] H. Ringertz, Acta Crystallogr. B 27 (1971) 285.
[22] Z.Kacar, Graduate School of Natural and Applied Sciences, M.Sc. Thesis, Dokuz Eylül University, İzmir, 2004.
[23] M.S. Refat, S.A. El-Korashy, A.S. Ahmed, Spectrochim. Acta A 70 (2008) 840.
[24] A.D. Becke, J. Chem. Phys. 98 (1993) 5648.
[25] C. Lee, W. Yang, R.G. Parr, Phys. Rev. B 37 (1988) 785.
[26] J.B. Foresman, E. Frisch, Exploring Chemistry with Electronic Structure Methods: A Guide to Using Gaussian, Gaussian, Pittsburgh, PA, 1993.
[27] NIST Chemistry Webbook, IR database, http://srdata.nist.gov/cccbdb.
[28] J. Baker, A.A. Jarzecki, P. Pulay, J. Phys. Chem. A 102 (1998) 1412.
[29] R. Ditchfield, J. Chem. Phys. 56 (1972) 5688.
[30] K. Wolinski, J.F. Hinton, P. Pulay, J. Am. Chem. Soc. 112 (1990) 8251.
[31] E. Runge, E.K.U. Gross, Phys. Rev. Lett. 52 (1984) 997.
[32] M. Petersilka, U.J. Gossmann, E.K.U. Gross, Phys. Rev. Lett. 76 (1966) 1212.
[33] R. Bauernschmitt, R. Ahlrichs, Chem. Phys. Lett. 256 (1996) 454.
[34] C. Jamorski, M.E. Casida, D.R. Salahub, J. Chem. Phys. 104 (1996) 5134.
[35] M.J. Frisch, Gaussian 03, Revision B.4, Gaussian Inc., Pittsburgh, PA, 2003.
[36] M. Silverstein, G.C. Basseler, C. Morill, Spectrometric Identification of Organic Compounds, Wiley, New York, 1981.
[37] N. Sundaraganesan, S. Ilakiamani, B.D. Joshua, Spectrochim. Acta A 67 (2007) 287.
[38] D. Lin-Vien, N.B. Colthup, W.G. Fateley, J.G. Grasselli, The Handbook of Infraredand Raman Characteristic Frequencies of Organic Molecules, Academic Press, Boston, MA, 1991.
[39] N. Sundaraganesan, H. Saleem, S. Mohan, Spectrochim. Acta A 59 (2003) 2511.
[40] M. Karabacak, M. Kurt, Spectrochim. Acta A 71 (2008) 876.
[41] M. Karabacak, M. Kurt, M. Cinar, A. Coruh, Mol. Phys. 107 (3) (2009) 253.
[42] H.O. Kalinowski, S. Berger, S. Braun, Carbon-13 NMR Spectroscopy, John Wiley and Sons, Chichester, 1988.
[43] K. Pihlaja, E. Kleinpeter (Eds.), Carbon-13 Chemical Shifts in Structural and Sterochemical Analysis, VCH Publishers, Deerfield Beach, 1994.
[44] C.H. Wu, A. Ramamoorthy, L.M. Gierasch, S.J. Opella, J. Am. Chem. Soc. 117 (1995) 6148.
[45] A. Ramamoorthy, C.H. Wu, S.J. Opella, J. Am. Chem. Soc. 119 (1997) 10479.
[46] K. Fukui, Science 218 (1982) 747.
[47] W. Barnum, J. Inorg. Nucl. Chem. 21 (1961) 221.
[48] R.H. Holm, F.A. Cotton, J. Am. Chem. Soc. 80 (1958) 5658.
[49] F.A. Cotton, C.W. Wilkinson, Advanced Inorganic Chemistry, 3rd edn, Interscience Publisher, New York, 1972.